A Novel Controlling System for Smart Farming-based Internet of Things (IoT)

Dodi Yudo Setyawan[1], Warsito[2]*, Roniyus Marjunus[3], Sumaryo[4]
Doctoral Program of Mathematics and Natural Sciences, Lampung University[1]
Department of Computer System, Faculty of Computer Science, Institute Informatics and Business Darmajaya[1]
Department of Physics, Faculty of Mathematics and Natural Sciences, Lampung University[2, 3]
Department of Agribusiness, Faculty of Agriculture, Lampung University[4]
Jl. Sumantri Brojonegoro No. 01, Gedong Meneng, Kec. Rajabasa, Kota Bandar Lampung (0721) 704946[1, 2, 3, 4]

***Abstract*—The integration of IoT systems in agriculture has become a very important need amid the high population and increasingly limited farmland, which demands researchers to be more innovative in addressing these issues. Using IoT systems for automatic irrigation, fertilization, and cooling based on sensor values through internet networks. Poor internet connection leads to the failure of automation and sustainability in online conditions, which can be very dangerous for plants. This paper presents a new IoT-based control system divided into two parts: an automation system and an IoT system, which can maintain sustainability in online conditions to ensure that plants in the planting area are always controlled. In addition, the sensors used have undergone calibration processes to determine the increase in precision of the sensor values produced. The research results show that the system can maintain sustainability under online conditions. Mobile apps are available for control when the system is online, but if it goes offline and is unable to reconnect, the Arduino Mega will fully manage control using soil moisture sensor values for irrigation processes if the values fall below a certain threshold. This demonstrates the sustainability of the system in online conditions, allowing continuous control and reducing the risk of plant death in the planting area. The calibration result shows an increase in precision for the air temperature and humidity (DHT 11 sensor) by 7.14 and 6.15, respectively. Additionally, the precision improvement for the soil pH sensor is 1.81, while for the soil moisture sensor and the water flow sensor, it is 0.13 and 0.008, respectively.**

***Keywords*—IoT; agriculture; automation; sustainability**

I. Introduction

The increasing population and shrinking agricultural land, as well as the increasing need for food, demand researchers to be more innovative in addressing these issues. In smart agriculture, researchers have a way of integrating IoT systems in the field of agriculture. The IoT system is used for automatic scheduled irrigation, fertilization, cooling, or sensor value-based. The system can perform tasks automatically by loading or uploading data to and from a database located in the cloud. If there is an internet network problem (offline), the automatic process will not run, and this situation can be very dangerous for plants. In general, the IoT system is unable to reconnect automatically to the internet network after a network problem occurs (offline), and this is a fundamental problem in integrating IoT systems in the field of agriculture. This study offers a new control system for smart agriculture based on IoT and addresses the research gap that the IoT system does not have full control over the entire system but rather serves as a tool to control and monitor planting areas so that the system's sustainability is ensured in online or on conditions and automation is maintained [1].

Specifically in urban areas, the construction of high-rise buildings continues to be carried out. The rooftops of these buildings can be utilized as farming areas for smart agriculture by installing greenhouses equipped with pipes and irrigation hoses, as seen in the following Fig. 1.

Fig. 1. Greenhouse on the rooftop

The greenhouse on the third floor, at a height of 12 meters, is located on campus at IBI Darmajaya at coordinates (-5.3774079, 105.2474507) as a place for research. The planting area in the greenhouse is divided into two with sizes of 8 x 13 meters and 8 x 10 meters, both in one control system. There are two air ventilators equipped with exhaust fans in each greenhouse. Each ventilator has a size of 0.5 x 0.5 meters. There are 160 polybags containing a mixture of soil and fertilizer used as planting media, each polybag is provided with water and liquid fertilizer channels using drip hoses. Each plant in the polybag is connected to pipes and hoses as irrigation and fertilization channels. In addition to offering a new control system for IoT-based smart agriculture, this research also offers a new mobile app for control and monitoring of agricultural areas in the greenhouse. Other researchers still use websites [2]-[7]. This will make it difficult for users to use the system, especially considering that the users are still very unfamiliar

with websites. Meanwhile, the control and monitoring that already use mobile applications [8]-[11], according to the researchers, still require improvements in the system.

IoT is a new field in the information technology and communication industry that connects almost everything to the internet. On the other hand, automation is a continuous cycle process that runs without manual intervention until the operator decides to stop the process. In theory, two approaches can be applied in smart farming, namely automation and IoT. In general, IoT systems are shown in Fig. 2 as follows.

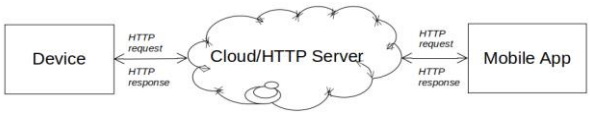

Fig. 2. General system IoT [14], [15]

The automation system can be seen in Fig. 3, and the integration of both to maintain the sustainability of the system is an initial hypothesis to be presented in the results of this research. The device section is divided into two parts, the first part is for the automation system, and the other part is used for the IoT system.

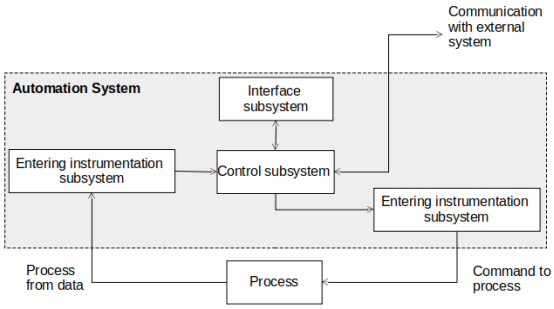

Fig. 3. Automation system [16]

There are mobile apps or websites used by users to monitor and control devices through the cloud. Devices can be in the form of a nodeMCU as the controller for sensors or actuators. There are two ways to communicate with devices on the node, namely through the Message Queue Telemetry Transport (MQTT) model [17] and Hypertext Transfer, which Protocol (HTTP) [18]. This study focuses on HTTP protocol communication and will divide the IoT system into two parts, namely the automatic system and the IoT system.

II. Related Works

In IoT, system security is very important to ensure that data from sensors and users is sent and read properly. Network security systems in IoT from the hardware side use the hardware platform security Advisor (IoT HarPSecA) framework, which can be used safely and easily with the elimination of security requirements and good security practices [19]. In addition to hardware security, network security from the network side using the provenance-based network layer forensics IoT (ProvMNet-IoT) method produces the best value when compared to other methods [20]. When encapsulation and extensible markup language (XML) methods are used to communicate between sensor nodes and actuators, data loss drops by 1.53% between nodes and 0.4% between the gateway and the server [21]. The improper selection of routes during data transmission between nodes is one of many factors that affect data loss. Besides data loss, the energy required also increases. This energy efficiency can be reduced using the Incremental Grey Wolf Optimization (IGWO) and Expanded Grey Wolf Optimization (Ex-GWO) methods [22]. Improving the Adaptive Data Rate (ADR) mechanism to enable cellular LoRa increases the performance of long-range wide area (LoRA) connectivity by up to 520% [23]. Finding strange data on wireless sensors using the DLSHiForest method based on Locality-Sensitive Hashing and the time window technique works more accurately and quickly than other methods [24]. To maintain privacy and user device collaboration in the cloud, the implementation of the Hierarchical Data Sandboxing module can maintain hierarchically organized application data [25]. The use of fog computing only reduces the time delay of control and monitoring processes, so this automation integration will have a better impact than fog computing [26].

The greenhouse is not always located in agricultural areas or on the rooftops of buildings, it can also be placed in coastal areas, Of course, the provision of freshwater as a source of plant nutrition in the greenhouse must be available. The process of converting seawater into fresh water for plant needs is also carried out. To achieve production efficiency, the prediction of this water production also needs to be done well by applying the Copula Bayesian Average Model (CBMA), where the Root Mean Square Error (RMSE) value is 40% [27]. Monitoring nutritional deficiencies in plants using a system engineering approach produces a dependability value of 0.9, indicating a very good confidence level in the monitoring system [28]. The precise use of water in the greenhouse is very important, To achieve this, the Decision Support System for Precision Irrigation (DSSPIM) can be implemented, and by applying this system, water usage for irrigation can be saved by 20% [29], Using evaporative cooling, compare two greenhouses, one of which is modified, resulting in a 40% water savings [30]. Another method to optimize irrigation in the greenhouse using recirculation (RC), with an efficiency obtained of 44–93% [31]. In addition to irrigation efficiency, the emission of irrigation from research that has been carried out produces the right recommendations in the irrigation or fertilization process so as not to have a negative impact on the environment [32]. The sensors used to determine the results of the irrigation process are soil moisture sensors, one of which uses semi-empirical soil moisture [33]. A multimodal neural network to estimate plant water stress can increase the accuracy of plant water stress estimation by 21% [34].

The optimal agricultural results from the greenhouse farming process are highly desirable for every farmer, which can be achieved through efficient energy use in the greenhouse. Various methods and models are used to obtain efficiency through modeling so that the right controllers can be applied in the greenhouse to achieve efficiency. Modeling with parameters such as internal greenhouse temperature and solar radiation shows a 24–34% reduction in efficiency. The application of Perception Model Representing (PMR) shows an RMSE value of 7.7–16.57% for energy prediction. Maximizing the plant photosynthesis process in the greenhouse by adding Light Emitting Diode (LED) light instead of using lamp light

results in an energy efficiency of 10–25%. In areas with extreme heat, cooling the greenhouse using a pressure droplet system achieves an efficiency value that is 6.9 times smaller compared to cooling with a chiller. In addition to adding LED light to enhance photosynthesis, CO_2 enrichment is also done. Local enrichment is 4.4 times more effective in terms of efficiency compared to overall enrichment. By comparing conventional open-field farming with soil-based and hydroponic greenhouse cultivation, we can see that CO_2 production in vertical farming is 5.6 to 16.7 times higher than in conventional farming in baseline scenarios and 2.3 to 3.3 times higher in alternative scenarios [40].

The use of photovoltaics can also generate energy efficiency each year, with photovoltaics producing 3,705 kWh of energy for greenhouse needs [41]. Using a multi-layer Feature Model can also reduce energy consumption [42]. Desalination systems and greenhouses for air, soil, plants, and land can generate around 85% of the water needed for tomato growth while also reducing cooling loads by more than 25% [43]. Utilizing an open-field and high-tech greenhouse systems approach can help reduce energy needs [44]. Airflows in a rooftop greenhouse (iRTG) produce harvested heat energy that can circulate into buildings with integrated HVAC systems, totalling 205.2 kWh/m2y1. [45].

Various methods for predicting greenhouse temperature and humidity to facilitate decision-making in maintaining greenhouse stability have been conducted by many researchers, including studies applying one-dimensional transient energy balance methods [46], the thermal performance of a 3D tomato model with a temperature prediction and real-time difference of around 5o Kelvin [47], using Gradient Boost Decision Tree with an RMSE value of 0.645 [48], and a combination of water curtains and liquid foam [49], using Tiny Machine Learning for microclimate in greenhouses, resulting in an average accuracy of 97% [50]. A greenhouse lighting model for supplementary lighting using LED with the Synthetically Active Radiation method resulted in an RMSE value of 5.5% [51]. A computation model for maintaining network connectivity in IoT systems is with a hybrid fault tolerance model with an accuracy level of 12.9% [52]. Thermoelectric generator (TEG) modules utilize thermal energy generated in greenhouses to produce electricity as an alternative energy source for IoT systems, with TEG producing an optimal voltage of 3 volts [53]. Manual and automatic irrigation controllers using Arduino and NRF24L01 sensor-based IoT systems are believed to save recruitment budget and increase productivity for farmers in managing agricultural crops [54], [55]. IoT systems using ESP32 can be used as weather stations to monitor air quality, with air quality data stored in text files [56]. IoT server integration based on cloud fog application placement strategies can reduce costs and energy consumption [57]. Two-way non-orthogonal multiple access (TW-NOMA) gives faster data rates [58]. A simulation of an IoT network's dual access scheme based on user groups demonstrates this.

Agriculture in a greenhouse with a closed environment with insect nets will not be immune to pest attacks, although the likelihood is lower compared to agriculture outside the greenhouse. Several types of pest attacks and control methods are used. For example, depthwise convolutional networks can find the Red Palm Weevil (RPW) with a 95.70% ± 1.46% accuracy [59], and the proposed deep learning Faster Regions with Convolutional Neural Networks (R-CNN) has the best recognition accuracy at 99.0% [60]. An early warning system for pest attacks on cucumber downy mildew using experimental evaluation method based on weather forecast input is implemented [61].

Researchers have also extensively studied the integration of machine learning in smart farming. Machine learning is artificial intelligence related to identifying patterns in data and using those patterns to make predictions about unseen data [62]. In other words, computer programs that are built to automatically improve their abilities with experience or learning. Decision tree is an algorithm used for decision-making where each option branches out. The shape or structure of a decision tree has roots and leaves like a tree, but upside down, where the root is at the top and the leaves are at the bottom. The use of decision trees to classify data classes allows accurate predictions of target classes from various data. Decision trees have rules, and each rule represents a different way from the root to each leaf. These rules are also called algorithms that have been developed based on decision trees. [63].

III. METHOD

The IoT sustainability system, whether online or on condition, is very important to ensure that the plants in the greenhouse are kept under controlled and well-monitored conditions. In conventional IoT systems, to automatically activate the water pump in the process of watering the plants, data must be loaded from the database in the cloud, making the system heavily dependent on the stability of the internet network. If the internet network is in good and stable condition, smart farming automation in the greenhouse will work well. However, if the opposite is true, automation will not work properly, posing a serious threat to the plants in the greenhouse, especially if it is located on a rooftop.

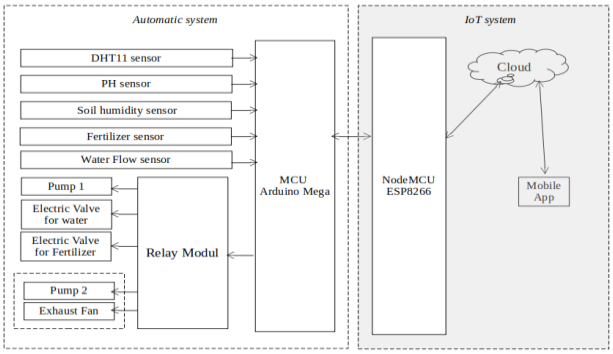

Fig. 4. System design

The new design of the control system is shown in Fig. 4, and each sensor is being calibrated to find out what its root mean square error (RMSE) is for the data from that sensor [64]. The RMSE formula serves as a metric for evaluating the performance of sensors in accurately measuring actual values.

$$RMSE = \sqrt{\frac{\sum_1^n (yi - \underline{yi})^2}{n}} \quad (1)$$

The formula for calculating sensor precision uses the RMSE of a series of measurements, where n stands for the quantity of samples or measurements, yi for the actual value (calibrator), and denotes the value the sensor measured. The standard approach to calculating sensor precision involves utilizing the RMSE derived from a series of measurements.

$$precision = \frac{1}{RMSE} \quad (2)$$

The new smart farming control system being offered uses two microprocessors. The first microprocessor on the Arduino Mega board controls the system automatically based on soil humidity sensor data, while the second microprocessor on the ESP8266 board is used for the IoT system connected to the cloud and mobile app. Both microprocessors communicate. Serially, and each microprocessor works independently. The flowchart of the automatic system on the Arduino Mega microprocessor is shown in Fig. 5 as follows.

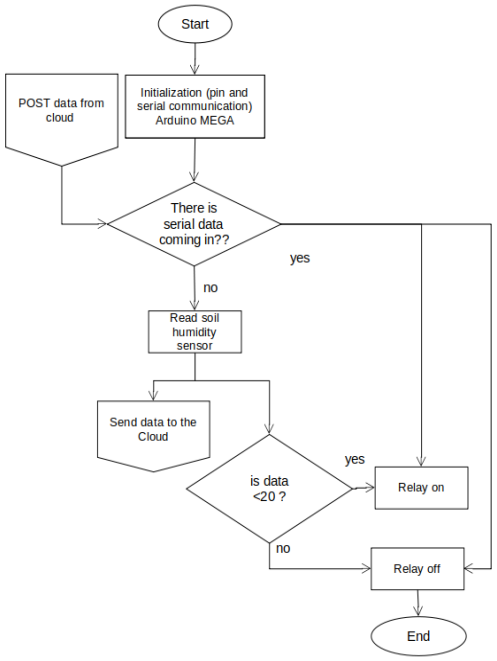

Fig. 5. Automatic system design

Initialization of the pins used as sensor data paths and serial data communication from other microprocessors is done during the initial setup of the microprocessor. If there is data in the microprocessor's serial buffer requested from the HTTP server, the microprocessor will command the relay module to turn on or off according to the relay number instructed. However, if there is no data, the microprocessor will read data from each sensor, and the relay will turn on or off according to the predetermined threshold. The threshold used is the soil moisture sensor, which has a humidity range of 20% to 80% [64]-[66].

The algorithm on the HTTP server can be seen in Fig. 6. POST and GET are sent and received from the mobile app and NodeMCU ESP8266. HTTP GET from NodeMCU is a request from NodeMCU to read data from the actuator relay database in an on or off condition according to the data in the database. HTTP POST from NodeMCU is a command to send data received by NodeMCU from Arduino Mega. This data is the entire value of the sensors that will be stored in the database.

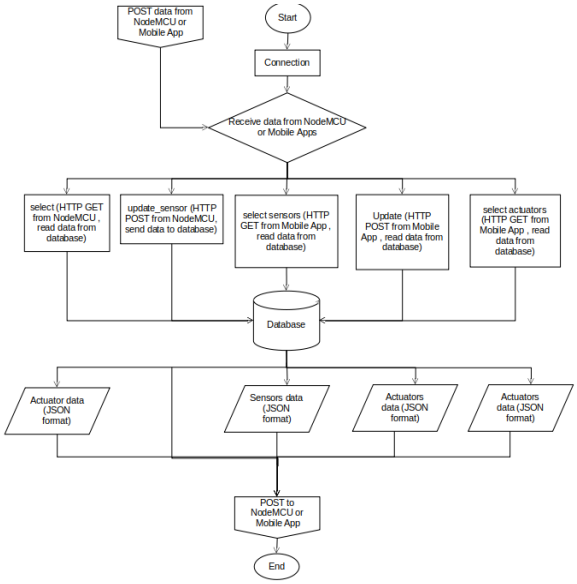

Fig. 6. Flowchart HTTP server

The algorithm on the mobile app can be seen in Fig. 7 below. From the server side, the GET command from the mobile app is a command to the server to send data from the database to the mobile app. To facilitate the mobile app receiving data from the server, the data is created in the form of Javascript Object Notation (JSON), both sensor data and actuator status data (in on or off condition). The POST command from the mobile app is to send commands to the server specifically to control the actuator.

Initialization of pin and serial communication is the first step in the NodeMCU flowchart. NodeMCU only acts as a bridge between automation systems and IoT, its task is only to receive and send data from and to the server or mobile app, with the addition of reconnecting procedures to the server.

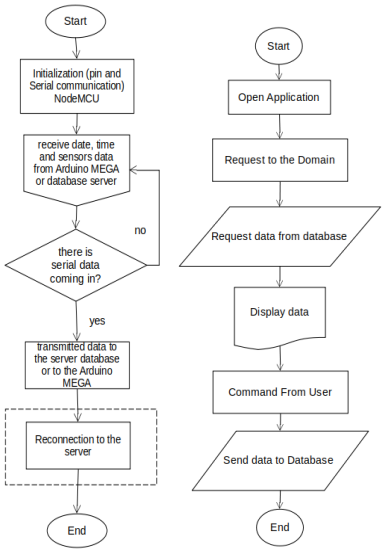

Fig. 7. Flowchart NodeMCU (a), flowchart mobile app (b)

Shortly after the mobile app is running, there is a request to the domain https://iot.darmajaya.ac.id, For each command POST and GET from the mobile app, the GET command will display data on the mobile app, either sensor value data or actuator status, while the POST command will send data about changing the actuator status from on to off or vice versa to the server.

Testing design of system sustainability to determine the sustainability of the internet network connectivity system, the data status of the connection between NodeMCU and Arduino Mega is sent to the computer via two USB ports. NodeMCU and Arduino Mega communicate serially. NodeMCU performs reconnection to the server to maintain the system's online status and sends the connection data to Arduino Mega. The Arduino Mega will operate in offline automation mode if an internet connection is not possible as seen in Fig. 8 below.

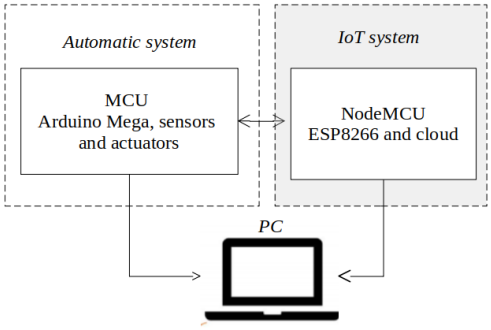

Fig. 8. Testing system sustainability

The connection between the Personal Computer and the Arduino Mega and NodeMCU is only done during system testing, after obtaining sustainability data, further connections will not be made again.

IV. Results and Discussion

This section presents the results and discussion of the new control system for smart agriculture based on IoT. The system consists of automation and IoT systems, the automation system uses an Arduino Mega MCU and the IoT system uses a NodeMCU 8266 wifi module for cloud connection. Sensors have been designed to measure temperature and humidity in the greenhouse, PH, humidity, and soil fertility. Water flow sensors are used to detect water flow in the pipes during watering and fertilizing processes. The fertilizer used is liquid AB Mix fertilizer. This detection is crucial to ensuring that both the control system and the IoT carry out the watering process correctly. Water and fertilizer are stored in separate tanks, there are four tanks in total, two tanks for liquid fertilizers A and B, one tank for the AB mix mixture, and another tank for water. The description of the components used can be seen in Fig. 9 as follows.

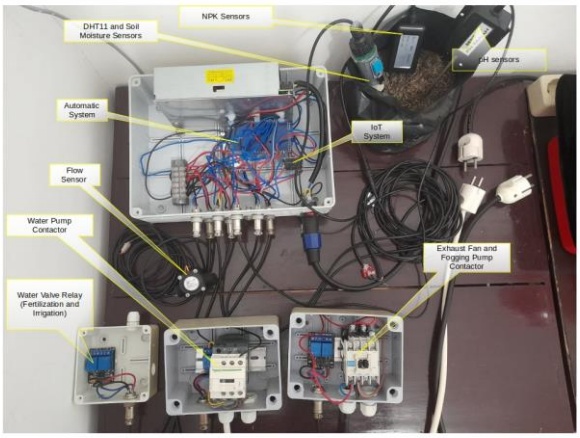

Fig. 9. System design results

Two contactors are added to assist the relay in switching the water pump and exhaust fan. The electrical power needed for the water pump ranges from 125 to 290 watts and the power needed for the exhaust fan ranges from 600 to 750 watts, so a contractor is needed for the switching process.

Temperature and humidity sensor DHT11 This sensor measures temperature between 0 and 5 degrees Celsius and relative humidity from 20% to 90%. The humidity accuracy level is ± 5% RH and ± 2°C. It has an 8-bit binary resolution. Response time is between 6 seconds and 15 seconds for humidity and 6 seconds and 30 seconds for temperature. Hysteresis value ± 1% RH and stability value ± 1% RH/year. Sensor output data in digital form consists of decimal and integral parts. The total data transmission is 40 bits, and the sensor sends higher data bits first. Data format: Data RH integral 8 bit + data RH decimal 8 bit + data T integral 8 bit + data T decimal 8 bit + checksum 8 bit. If the data transmission is correct, the checksum should be the last 8 bits of data RH integral 8 bit + data RH decimal 8 bit + data T integral 8 bit + data T decimal 8 bit. The power supply required 5 volts, and the current needed 0.5 mA to 2.5 mA. The internal structure of the sensor can be seen in Fig. 10. The parts of the sensor consist of lower and upper electrodes, a holding, and a glass substrate.

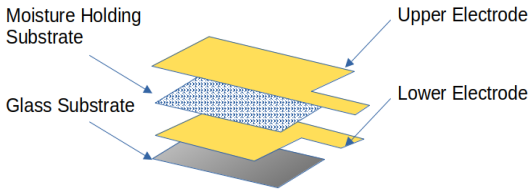

Fig. 10. Internal structure of DHT11 sensor

Calibration has been conducted to determine the linearity value of the DHT11 sensor in comparison to the calibrator (htc-1). This calibration involved collecting temperature data simultaneously with the object being monitored by the temperature and humidity sensors. Presented below are the calibration results for both the temperature and humidity sensor DHT11 and the calibrator data. Additionally, a graph illustrating the calibration of the air temperature sensor DHT11 is provided.

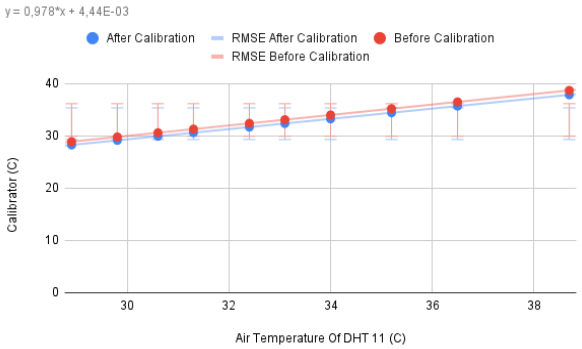

Fig. 11. Calibration graph (air temperature)

The linearity formula obtained from the calibration conducted is y = 0.978*x + 4.44E-03. Provided below is the calibration graph for the DHT11 humidity sensor.

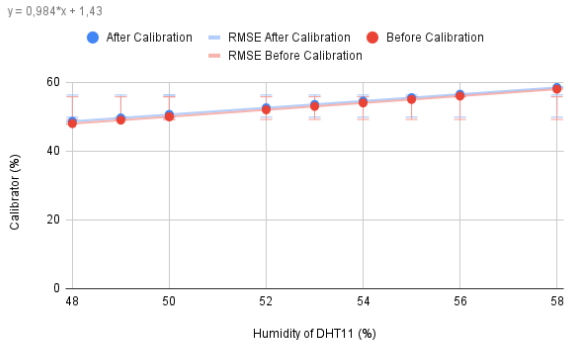

Fig. 12. Calibration graph (air humidity)

Following the calibration process, the linearity formula y = 0.984*x + 1.43 is derived. These formulas have been integrated into the source code to enhance precision. Below is a snippet of the source code:

```
value_of_DHT11=dht11.read(humi, temp);

float fix_humi = (0,984*humi) +1,43;

float fix_temp = (0,978*temp) +0,00444;
```

The graphs in Fig. 11 and 12 show a decrease in the RMSE value following the integration of the linearity formula into the source code, declining from 0.74 to 0.11.

Soil Moisture Sensor SEN0193 Capacitive Soil Moisture Sensor exploits the dielectric contrast between water and soil, where dry soil has a relative permittivity between 2 and 6 and water has a value around 80. A capacitive soil moisture sensor uses the principle of a capacitor to estimate the water content in the soil. The amount of charge that a material can store at a specific electrical potential is what is known as capacitance [68]. Generally, a capacitor is visualized as a parallel plate configuration similar to the one shown in the Fig. 13.

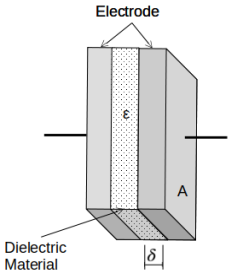

Fig. 13. Parallel plate

The surface integral between the electric field E and the dielectric material with relative permittivity ε crossing the area of the capacitor surface is used to define charge Q. The definition of electric potential V is defined using the line integral of the electric field. For parallel plate capacitors, it is assumed that the electric field is constant across the entire dielectric surface, which is the common relationship between the geometric properties of parallel plate capacitors and the dielectric material present in the capacitor. Capacitance measured by a soil moisture sensor is different from parallel plate capacitors because the capacitor plates are not parallel, but planar. This means that the plates are adjacent to each other, not above each other; and the dielectric material is soil, not a thin layer pressed between the plates. This is visually illustrated in Fig. 14 below:

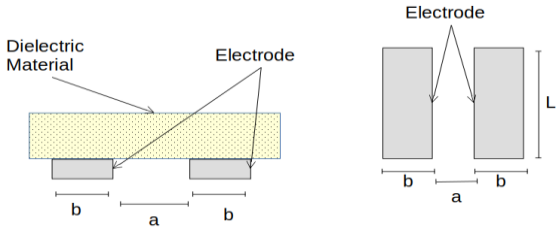

Fig. 14. Soil moisture sensor

It can be seen that the sensor electrode acts as a capacitor plate, both exposed to dielectric material and assumed to be dry or wet soil. Capacitive soil moisture sensors are paired with the IC 555 timer circuit and produce the design cycle of the internal sensor circuit. The water condition in the soil is described in terms of the amount of water and energy associated with the force holding water in the soil. Water potential is the energy state of the water, and water content determines the amount of water. Plant growth, soil temperature, chemical transport, and groundwater recharge all depend on the water conditions in the soil. Although there is a unique relationship between water content and water potential for a particular soil, these physical properties describe the water condition in the soil differently. It is important to understand the differences when choosing a soil moisture measuring device. Soil water content is expressed gravimetrically or volumetrically. Gravimetric water content (θg) is the mass of water per unit mass of dry soil. Measurements are taken by weighing a soil sample (M wet), drying the sample to remove the water, and then weighing the dried soil (M dry).

$$\theta g = \frac{M\ water}{M\ soil}$$

$$= \frac{M\ wet - M\ dry}{M\ dry} \quad (3)$$

The volumetric water content (θv) is the volume of liquid water per unit volume of soil. Volume is the ratio of mass to density (ρ) that is given:

$$\theta v = \frac{Volume\ water}{Volume\ soil}$$

$$= \frac{M\ water}{\rho\ soil} \times \frac{\rho\ water}{M\ soil}$$

$$= \frac{\theta g \times \rho\ soil}{\rho\ water} \quad (4)$$

Bulk density (ρbulk) is used for soil and is the ratio of the dry mass of A capacitive to the sample volume. Water density is close to 1 and is often overlooked. Another useful property, soil porosity (ε), is related to bulk density, as shown by the following expression:.

$$\varepsilon = 1 - \frac{\rho bulk}{\rho\ soil} \quad (5)$$

The term ρ dense refers to the density of the solid fraction of soil and is approximated to be 2.6 g/cm3. Water flux: the movement of water occurs within the soil profile, between soil and plant roots, and between soil and atmosphere. As in all natural systems, the movement of a material depends on the energy gradient. Groundwater potential is an expression of the energy state of water in the soil and must be known or estimated to describe water flux. Water molecules in the soil matrix are subject to various forces. If there are no adhesive forces, water molecules will move through the soil at the same speed as in free air, minus the delay from collisions with solid materials such as sand through a sieve. Groundwater potential contributes to adhesive and cohesive forces and describes the energy status of groundwater. The fundamental forces acting on groundwater are gravity, matrix, and osmotic. Water molecules have energy based on their position in the gravitational force field, as all materials have potential energy. The gravitational potential component of the total water potential is what describes this energy component. Here is the calibration for the SEN0193 soil moisture sensor.

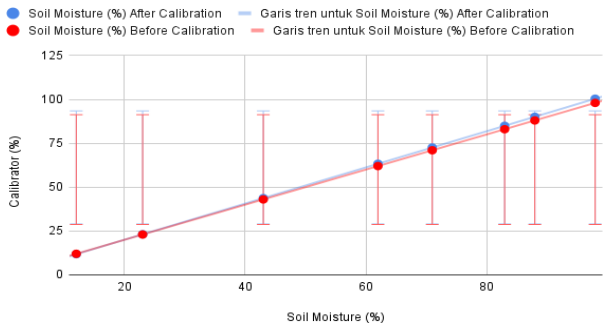

Fig. 15. Calibration graph soil moisture sensor

Following the calibration process, the linearity formula y = 0.521*x + 14.6 is obtained. This formula has been incorporated into the source code to enhance precision. Below is a snippet of the source code.

```
float soil_ moisture_ value = analogRead(pinKelem_tanah);

float stable_soil_moisture_value = constrain(soil_ moisture_ value,200,700);

float value = (((stable_soil_moisture_value-200)/500)*100);

float fix_velue = (0,521 * value) +14,6;
```

The graphs in Fig. 15 depict a decrease in the RMSE value subsequent to integrating the linearity formula into the source code, reducing from 2.34 to 1.77. This indicates an enhancement in measurement precision.

The potential gravitational effect is easily seen when the attractive force between water and soil is smaller than the gravitational force acting on water molecules and water flows downward. The arrangement of solid soil particle matrices produces capillary and electrostatic forces and determines the potential matrix of soil water. The magnitude of the force depends on the texture and physicochemical properties of solid soil materials. Most methods for measuring soil water potential are only sensitive to matrix potential. Soil water is the solution. The polar nature of water molecules results in their interactions with other electrostatic poles present in the solution as free ions. The energetic status component is osmotic potential. Methods for measuring soil water matric potential include tensiometers, thermocouple psychrometers, electrical conduction, and heat dissipation methods such as the Campbell Scientific 229 sensor model. There is a unique relationship between water content and water potential for each soil. The characteristic curve of water in soil for three soils is shown below. For a specific water potential, the finer the soil texture, the more water is retained in the soil. Coarse-textured soils, like sand, consist mostly of large, empty pores that do not hold water when subjected to relatively small forces. Fine-textured soils have a wider distribution of pore sizes and larger particle surface areas. As a result, a greater change in water potential is needed to extract the same amount of water. A larger surface area means more water is absorbed through electrostatic forces.

The real-time sensor data results within a specific time range. The DHT11 and SEN0193 sensors mentioned above have the same range of data for air temperature, air humidity, and soil moisture, ranging from 0 to 100. Therefore, real-time data monitoring is displayed in one graph on the website, including the monitoring of the three sensor values (Fig. 16).

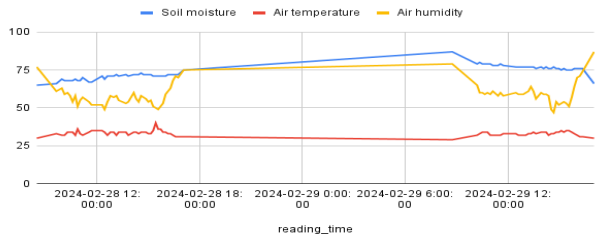

Fig. 16. Monitoring data sensor DHT11 and soil humidity

The air temperature at 12:00 during the day is higher compared to 18:00 until 06:00, however, the value of air humidity and soil humidity are inversely related to the air temperature value. This is because there is no evaporation

process, which has a greater value occurring at 12:00 compared to 18:00 until 06:00.

A. Soil pH Sensor

The measurement range of Power of Hydrogen (pH) or acidity or alkalinity level of soil is between 3.5 and 8. This sensor requires a power supply voltage between 3 volts and 4.7 volts and an analog output value between 4 and 4.5 volts. The response time is 0.1 seconds to 0.3 seconds, and the sensitivity level is 0.036 volts to 0.234 volts. Below is the calibration for the soil pH sensor. Using the Digital Soil Analyzer calibrator.

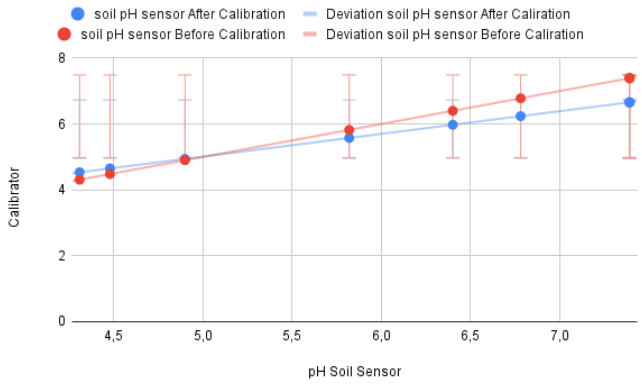

Fig. 17. Calibration graph soil pH sensor

Following the calibration process, the linearity formula y = 1.22*x - 0.98 is obtained. This formula has been integrated into the source code to enhance precision. Below is a snippet of the source code.

```
float Soil_pH_sensor_value = analogRead (sensorPh);

float outputValue = (-0.0693*nilaisensorPh)+7.3855;

float value_pH = constrain(outputValue, 0, 100);

float fix_value_pH = (1,22*nilai_ph)-0,984;
```

The graph in Fig. 17 shows a decrease in the RMSE value subsequent to integrating the linearity formula into the source code, decreasing from 0.54 to 0.27. This signifies an improvement in measurement precision.

The application of liquid fertilizer tends to elevate soil pH due to its acidic properties, typically having pH values below 7. When the initial pH is less than 7.38, it tends to decrease further during the fertilization process. However, as the plants absorb the fertilizers as nutrients, the pH gradually rises over time.

B. Nitrogen Phosphorus Potassium (NPK) Sensor

The measurement range is between 0 and 1999 mg/kg, with a response time of less than 1 second. The communication port uses RS485 with baud rates of 2400, 4800, and 9600 bits per second. The voltage required is between 12 and 24 volts. Asynchronous communication protocol uses differential signal techniques to transfer binary data from one device to another with positive voltage values of 5 volts and negative 5 volts. In addition, communication is done in a half-duplex with a maximum speed of 30 Mbps, and a distance range of up to 1200 meters. The value of each element N, P, and K will increase along with the fertilization process, and these values will also decrease after nutrient uptake by the plants. The values of each element will also be proportional, either decreasing or increasing, with respect to soil pH. The graph of NPK sensor values in mg/kg units can be seen in Fig. 18 as follows.

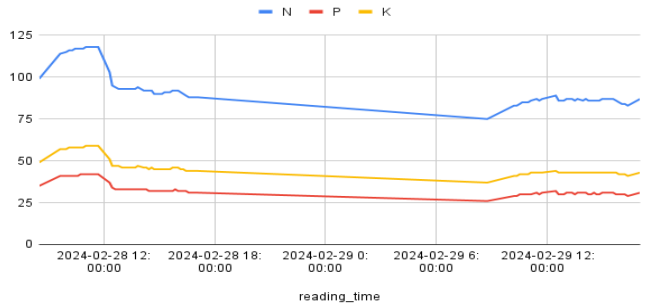

Fig. 18. NPK values

The NPK values experience an increase during fertilization and a decrease during the absorption process by plants or the irrigation process. The solubility of NPK values in irrigation water is to blame for this. The NPK values experience simultaneous increases and decreases.

C. YF-S201 Sensor

The YF-S201 type water flow sensor is a commonly used water flow sensor in various applications, especially in measuring water flow in monitoring and control systems. The working principle of this sensor is based on the Hall effect, which utilizes a magnetic field to detect the movement of charged particles such as water. When water flows through the sensor, the rotor inside it rotates. The rotor has a permanent magnet inside. When the rotor rotates, its magnetic field changes, which is then detected by the Hall sensor to produce an output signal correlated with the water flow rate (Fig. 19).

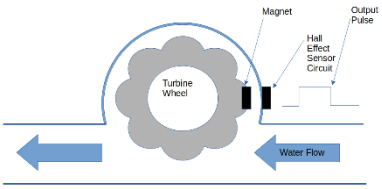

Fig. 19. Sensor YF-S201 diagram

When a magnetic field is applied perpendicular to the electric current flowing in a conductor, the magnetic field will push the electrons in a direction perpendicular to both the magnetic field and the electric current. Due to the interaction between the magnetic field and the electron charge, electrons flowing in the direction of the electric current will experience deflection. This Lorentz force causes the electrons to accelerate in a direction perpendicular to both fields, resulting in a collection of positive and negative charges on the sides of the conductor. This collection of charges creates an electric potential difference between the two sides of the conductor, perpendicular to the direction of the electric current. This potential difference is known as the Hall potential, and its magnitude is proportional to the strength of the magnetic field, electric current, and distance between the two sides of the

conductor. The Hall potential can be measured using a Hall sensor, which is a semiconductor device sensitive to magnetic fields. When a magnetic field is applied, the Hall sensor will produce an output voltage proportional to the Hall potential occurring in the conductor. By measuring this output voltage, we can obtain information about the strength of the magnetic field, electric current, or even the characteristics of the conductive material. This principle can be integrated into a sensor diagram to measure the flow rate of water or other fluids. Below is the calibration for the YF-S201 sensor.

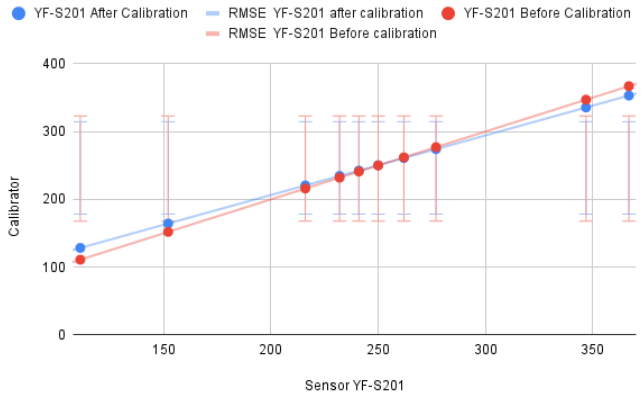

Fig. 20. Calibration graph of the YF-S201 sensor

Following the calibration process, the linearity formula y = 0.898*x + 26.7 is obtained. This formula has been implemented into the source code to enhance precision. Below is a snippet of the source code.

```
Calc = (TURBINE * 60 / 7.5);

float fix_Cals = (0,898*x)+26,7;
```

The graph in Fig. 20 illustrates a decrease in the RMSE value after integrating the linearity formula into the source code, decreasing from 18.41 to 11.27. This signifies an enhancement in measurement precision (Fig. 21).

Fig. 21. Rate sensor YF-S201 data flow

The flow rate increases to a certain value during irrigation and fertilization and returns to 0 when finished. In addition to soil humidity data, the increase in flow rate data is used as feedback during irrigation and fertilization. Feedback like this is not found in other IoT smart farming systems. Success in the irrigation and fertilization processes must be known precisely. Failure in this process results in a lack of soil humidity and nutrients, which can lead to plant death. The Arduino Mega microprocessor is fully in control of this controller. The main microprocessor of the Arduino Mega 2560 Rev3 board is the ATmega2560 chip, which operates at a frequency of 16 MHz. It consists of input and output lines to connect to many external devices. At the same time, operation and processing are not slow due to the much larger RAM than other processors. The board is also equipped with the ATmega16U2 USB Serial processor, which serves as an interface between the USB input signal and the main processor. The board consists of 16 analog input pins and 22 digital inputs. The microprocessor communicates serially with the NodeMCU ESP8266. The NodeMCU ESP8266EX 32-bit microcontroller (MCU) RSIC 16-bit. The CPU speed is 80 MHz up to a maximum of 160 MHz with the Real-Time Operating System (RTOS). 20% of the Microprocessor without Interlocked Pipeline Stages (MIPS) is occupied by the WiFi stack, the rest can be used for programming and user application development. The Random Access Memory (RAM) size is less than 36 kB when ESP8266EX operates in router-connected mode, with programmable space accessible around 36 kB. External Flash SPI is used together with ESP8266EX to store the program's theoretical memory capacity of up to 16 MB. The firmware has access to 17 GPIO pins for use in various functions. These pins are multiplexed with other functions such as I2C, I2S, UART, PWM, IR Remote Control, etc. The I/O soldering of I/O data is bi-directional and tri-state, which includes input and output data control buffers. In addition, I/O can be set to a special and fixed state. For example, if you want to reduce chip power consumption, all data input and output activation signals can be set to low-power standby. You can move some specific statuses into I/O. When I/O is not powered by an external circuit, I/O will remain in the last used state. Some positive feedback is generated by the remaining pin functions, therefore, the external drive power needs to be stronger than the positive feedback. Nevertheless, the driving energy required is around 5 uA.

Based on the obtained calibration data, calculations are then conducted using formula 2, resulting in an increase in precision, as shown in Fig. 22 below.

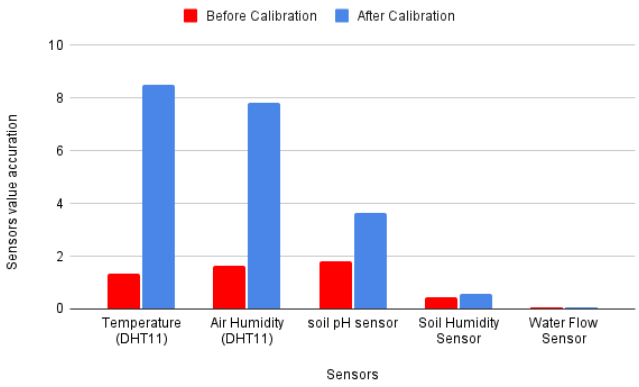

Fig. 22. Increase in precision

Applying the second formula, the precision improvement post-calibration for air temperature and humidity (DHT 11 sensor) is 7.14 and 6.15, respectively. For the soil pH sensor,

the increase is 1.81, while for the soil moisture sensor and the water flow sensor, it is 0.13 and 0.008, respectively.

D. Mobile Apps

Mobile apps are built using Android Studio with a user-friendly interface for controlling and monitoring farming (Fig. 23).

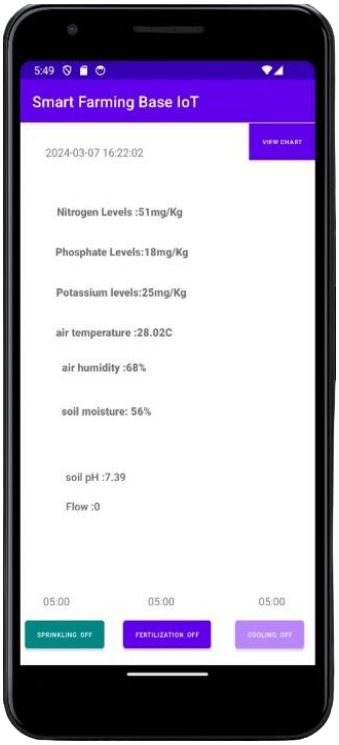

Fig. 23. Mobile apps

Mobile apps monitor sensor values (NPK, DHT11 sensor, soil humidity sensor, soil pH sensor, and Flow sensor) in real time during the farming process. The Mobile App also monitors the NodeMCU, whether it is online or offline, based on the visible time and date data. If the time and date data differs from the real-time data on the Android device, then the NodeMCU device is considered offline. Problems with the router device, server downtime, or internet network can all be the cause of this. In such cases, the user must fix the internet connectivity. The Arduino Mega will take over the automatic controller while it is in offline mode and automatically water the plants in accordance with the soil humidity sensor value to prevent plant death. To prevent forgetting to stop a command, the user in online mode performs the watering, fertilizing, and cooling processes within five minutes for each command.

E. Results of the Sustainability System Testing

POST instructions are used to send data from the NodeMCU device A to the cloud, while GET instructions are used to request data from the cloud. The server or cloud will respond with a decimal value of 200 if the POST or GET instructions are successful and the data is saved in the database. This value is used to indicate whether the NodeMCU is online or offline.

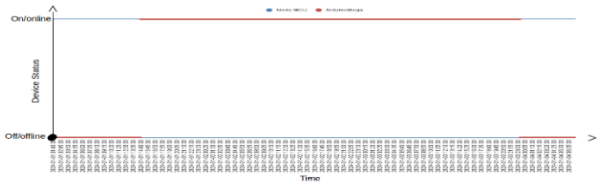

Fig. 24. The results of sustainability system testing

The NodeMCU and Arduino Mega are powered up simultaneously and establish communication. The NodeMCU initiates a POST command to transmit data to the server, and upon receiving a server response with a decimal value of 200, it indicates successful data entry into the database. Conversely, if the data fails to reach the server or encounters network issues, the server response decimal value is -1. These two scenarios determine the operational mode of the Smart Farming system, whether online or offline automation. A response of 200 triggers the NodeMCU to assume full control of the smart farming online automation system, overseeing watering, fertilization, and temperature control based on the database information. On the other hand, a server response of -1 prompts the NodeMCU to instruct the Arduino Mega to execute offline automation. Fig. 24 depicts the outcomes of the automation system operating alternatively in both online and offline modes between NodeMCU and Arduino Mega. When the internet network connection is stable, NodeMCU takes charge of the online automation system. However, in the event of an internet network issue, Arduino Mega takes over control and executes offline automation. The Arduino Mega, in offline automation mode, conducts parameter monitoring in the Smart Farming system, including sensor data for soil moisture levels.

V. Conclusion

The new control system for IoT-based smart agriculture in an experimental framework has shown improved control capabilities in agricultural areas. The system is able to maintain sustainability in online or on conditions. When online control can be done using mobile apps, but if offline control occurs and the system cannot reconnect, then control is fully done by Arduino Mega using soil moisture sensor values for the watering process if the value reaches the minimum limit. This shows the sustainability of the system in its current state so that control can continue to be carried out and reduce the risk of plant death in the planting area. In addition, calibration is also carried out on the DHT11 sensor for temperature parameters with a standard deviation of 0, soil humidity sensor SEN0193 with a standard deviation of 0.42, soil pH sensor with a standard deviation of 0.54, and the NPK sensor with a standard deviation of Nitrogen is 22.50. The standard deviation of phosphorus is 7.84, and the standard deviation of potassium is 8.36. The water flow sensor YF-S201 standard deviation is 19.94. Sensor calibration as a measuring tool must be done, this also applies to other IoT systems, which must show the standard deviation of the sensors used so that it can later be called precision farming with a certain standard deviation value.

Declaration of Competing Interest

The authors declare that they have no known competing financial interests or personal relationships that could have appeared to influence the work reported in this paper.

ACKNOWLEDGMENT

The authors would like to express special thanks for the constructive comments from the editor and reviewers, leading to significant and substantial improvements to the manuscript.

REFERENCES

[1] D. Y. Setyawan, W. Warsito, R. Marjunus, N. Nurfiana, and R. Syahputri, "A Systematic Literature Review: Internet of Things on Smart Greenhouse," *Int. J. Adv. Comput. Sci. Appl.*, vol. 13, no. 12, 2022, doi: 10.14569/IJACSA.2022.0131280.

[2] E. A. Abioye *et al.*, "IoT-based monitoring and data-driven modelling of drip irrigation system for mustard leaf cultivation experiment," *Inf. Process. Agric.*, vol. 8, no. 2, pp. 270–283, Jun. 2021, doi: 10.1016/j.inpa.2020.05.004.

[3] S. Pasika and S. T. Gandla, "Smart water quality monitoring system with cost-effective using IoT," *Heliyon*, vol. 6, no. 7, p. e04096, Jul. 2020, doi: 10.1016/j.heliyon.2020.e04096.

[4] H. Andrianto, Suhardi, A. Faizal, N. Budi Kurniawan, and D. Praja Purwa Aji, "Performance evaluation of IoT-based service system for monitoring nutritional deficiencies in plants," *Inf. Process. Agric.*, vol. 10, no. 1, pp. 52–70, Mar. 2023, doi: 10.1016/j.inpa.2021.10.001.

[5] J. Chigwada, F. Mazunga, C. Nyamhere, V. Mazheke, and N. Taruvinga, "Remote poultry management system for small to medium scale producers using IoT," *Sci. Afr.*, vol. 18, p. e01398, Nov. 2022, doi: 10.1016/j.sciaf.2022.e01398.

[6] W. A. Jabbar, T. Subramaniam, A. E. Ong, M. I. Shu'Ib, W. Wu, and M. A. de Oliveira, "LoRaWAN-Based IoT System Implementation for Long-Range Outdoor Air Quality Monitoring," *Internet Things*, vol. 19, p. 100540, Aug. 2022, doi: 10.1016/j.iot.2022.100540.

[7] Y. Liu *et al.*, "Integrated near-infrared QEPAS sensor based on a 28 kHz quartz tuning fork for online monitoring of CO2 in the greenhouse," *Photoacoustics*, vol. 25, p. 100332, Mar. 2022, doi: 10.1016/j.pacs.2022.100332.

[8] K. Koteish, H. Harb, M. Dbouk, C. Zaki, and C. Abou Jaoude, "AGRO: A smart sensing and decision-making mechanism for real-time agriculture monitoring," *J. King Saud Univ. - Comput. Inf. Sci.*, vol. 34, no. 9, pp. 7059–7069, Oct. 2022, doi: 10.1016/j.jksuci.2022.06.017.

[9] W. J. P. Kuijpers, D. J. Antunes, S. van Mourik, E. J. van Henten, and M. J. G. van de Molengraft, "Weather forecast error modelling and performance analysis of automatic greenhouse climate control," *Biosyst. Eng.*, vol. 214, pp. 207–229, Feb. 2022, doi: 10.1016/j.biosystemseng.2021.12.014.

[10] D. F. Parks *et al.*, "IoT cloud laboratory: Internet of Things architecture for cellular biology," *Internet Things*, vol. 20, p. 100618, Nov. 2022, doi: 10.1016/j.iot.2022.100618.

[11] [S. Zhang *et al.*, "Investigation on environment monitoring system for a combination of hydroponics and aquaculture in greenhouse," *Inf. Process. Agric.*, vol. 9, no. 1, pp. 123–134, Mar. 2022, doi: 10.1016/j.inpa.2021.06.006.

[12] O. Liberg, M. Sundberg, Y.-P. E. Wang, J. Bergman, and J. Sachs, "The Cellular Internet of Things," in *Cellular Internet of Things*, Elsevier, 2018, pp. 1–13. doi: 10.1016/B978-0-12-812458-1.00001-0.

[13] K. L. S. Sharma, "Why Automation?," in *Overview of Industrial Process Automation*, Elsevier, 2017, pp. 1–14. doi: 10.1016/B978-0-12-805354-6.00001-3.

[14] F. Khodadadi, "Chapter 1 - Internet of Things: an overview," 2017.

[15] N. Kefalakis, "Chapter 2 - Open source semantic web infrastructure for managing IoT resources in the Cloud," 2017.

[16] K. L. S. Sharma, "Automation System Structure," in *Overview of Industrial Process Automation*, Elsevier, 2017, pp. 15–23. doi: 10.1016/B978-0-12-805354-6.00002-5.

[17] J. Simla. A, R. Chakravarthy, and M. Leo. L, "An Experimental study of IoT-Based Topologies on MQTT protocol for Agriculture Intrusion Detection," *Meas. Sens.*, vol. 24, p. 100470, Dec. 2022, doi: 10.1016/j.measen.2022.100470.

[18] H. A. Méndez-Guzmán *et al.*, "IoT-Based Monitoring System Applied to Aeroponics Greenhouse," *Sensors*, vol. 22, no. 15, p. 5646, Jul. 2022, doi: 10.3390/s22155646.

[19] M. G. Samaila *et al.*, "Performance evaluation of the SRE and SBPG components of the IoT hardware platform security advisor framework," *Comput. Netw.*, vol. 199, p. 108496, Nov. 2021, doi: 10.1016/j.comnet.2021.108496.

[20] L. Sadineni, E. S. Pilli, and R. B. Battula, "ProvNet-IoT: Provenance based network layer forensics in Internet of Things," *Forensic Sci. Int. Digit. Investig.*, vol. 43, p. 301441, Sep. 2022, doi: 10.1016/j.fsidi.2022.301441.

[21] J. Wang, M. Chen, J. Zhou, and P. Li, "Data communication mechanism for greenhouse environment monitoring and control: An agent-based IoT system," *Inf. Process. Agric.*, vol. 7, no. 3, pp. 444–455, Sep. 2020, doi: 10.1016/j.inpa.2019.11.002.

[22] A. Seyyedabbasi, F. Kiani, T. Allahviranloo, U. Fernandez-Gamiz, and S. Noeiaghdam, "Optimal data transmission and pathfinding for WSN and decentralized IoT systems using I-GWO and Ex-GWO algorithms," *Alex. Eng. J.*, vol. 63, pp. 339–357, Feb. 2023, doi: 10.1016/j.aej.2022.08.009.

[23] V. Moysiadis, T. Lagkas, V. Argyriou, A. Sarigiannidis, I. D. Moscholios, and P. Sarigiannidis, "Extending ADR mechanism for LoRa enabled mobile end-devices," *Simul. Model. Pract. Theory*, vol. 113, p. 102388, Dec. 2021, doi: 10.1016/j.simpat.2021.102388.

[24] Y. Yang *et al.*, "Fast wireless sensor for anomaly detection based on data stream in an edge-computing-enabled smart greenhouse," *Digit. Commun. Netw.*, vol. 8, no. 4, pp. 498–507, Aug. 2022, doi: 10.1016/j.dcan.2021.11.004.

[25] Y. Yoon, "Chapter 3 - Device/Cloud collaboration framework for intelligence applications," 2017.

[26] A. V. Dastjerdi, "Chapter 4 - Fog Computing: principles, architectures, and applications," 2017.

[27] M. Ehteram, A. N. Ahmed, P. Kumar, M. Sherif, and A. El-Shafie, "Predicting freshwater production and energy consumption in a seawater greenhouse based on ensemble frameworks using optimized multi-layer perceptron," *Energy Rep.*, vol. 7, pp. 6308–6326, Nov. 2021, doi: 10.1016/j.egyr.2021.09.079.

[28] H. Andrianto, Suhardi, A. Faizal, N. Budi Kurniawan, and D. Praja Purwa Aji, "Performance evaluation of IoT-based service system for monitoring nutritional deficiencies in plants," *Inf. Process. Agric.*, p. S2214317321000792, Oct. 2021, doi: 10.1016/j.inpa.2021.10.001.

[29] C. M. Flores Cayuela, R. González Perea, E. Camacho Poyato, and P. Montesinos, "An ICT-based decision support system for precision irrigation management in outdoor orange and greenhouse tomato crops," *Agric. Water Manag.*, vol. 269, p. 107686, Jul. 2022, doi: 10.1016/j.agwat.2022.107686.

[30] I. Tsafaras *et al.*, "Intelligent greenhouse design decreases water use for evaporative cooling in arid regions," *Agric. Water Manag.*, vol. 250, p. 106807, May 2021, doi: 10.1016/j.agwat.2021.106807.

[31] F. Parada, X. Gabarrell, M. Rufí-Salís, V. Arcas-Pilz, P. Muñoz, and G. Villalba, "Optimizing irrigation in urban agriculture for tomato crops in rooftop greenhouses," *Sci. Total Environ.*, vol. 794, p. 148689, Nov. 2021, doi: 10.1016/j.scitotenv.2021.148689.

[32] C. van der Salm, W. Voogt, E. Beerling, J. van Ruijven, and E. van Os, "Minimising emissions to water bodies from NW European greenhouses; with focus on Dutch vegetable cultivation," *Agric. Water Manag.*, vol. 242, p. 106398, Dec. 2020, doi: 10.1016/j.agwat.2020.106398.

[33] A. K. Shakya, A. Ramola, A. Kandwal, and A. Vidyarthi, "Soil moisture sensor for agricultural applications inspired from state of art study of surfaces scattering models & semi-empirical soil moisture models," *J. Saudi Soc. Agric. Sci.*, vol. 20, no. 8, pp. 559–572, Dec. 2021, doi: 10.1016/j.jssas.2021.06.006.

[34] K. Wakamori, R. Mizuno, G. Nakanishi, and H. Mineno, "Multimodal neural network with clustering-based drop for estimating plant water stress," *Comput. Electron. Agric.*, vol. 168, p. 105118, Jan. 2020, doi: 10.1016/j.compag.2019.105118.

[35] A. Costantino, L. Comba, G. Sicardi, M. Bariani, and E. Fabrizio, "Energy performance and climate control in mechanically ventilated greenhouses: A dynamic modelling-based assessment and investigation," *Appl. Energy*, vol. 288, p. 116583, Apr. 2021, doi: 10.1016/j.apenergy.2021.116583.

[36] F. Mahmood, R. Govindan, A. Bermak, D. Yang, C. Khadra, and T. Al-Ansari, "Energy utilization assessment of a semi-closed greenhouse using

data-driven model predictive control," *J. Clean. Prod.*, vol. 324, p. 129172, Nov. 2021, doi: 10.1016/j.jclepro.2021.129172.

[37] D. Katzin, L. F. M. Marcelis, and S. van Mourik, "Energy savings in greenhouses by transition from high-pressure sodium to LED lighting," *Appl. Energy*, vol. 281, p. 116019, Jan. 2021, doi: 10.1016/j.apenergy.2020.116019.

[38] G. Zapalac, "Simulation of a convectively-cooled unventilated greenhouse," *Comput. Electron. Agric.*, vol. 193, p. 106563, Feb. 2022, doi: 10.1016/j.compag.2021.106563.

[39] Y. Zhang, D. Yasutake, K. Hidaka, T. Okayasu, M. Kitano, and T. Hirota, "Crop-localised CO2 enrichment improves the microclimate, photosynthetic distribution and energy utilisation efficiency in a greenhouse," *J. Clean. Prod.*, vol. 371, p. 133465, Oct. 2022, doi: 10.1016/j.jclepro.2022.133465.

[40] T. Blom, A. Jenkins, R. M. Pulselli, and A. A. J. F. van den Dobbelsteen, "The embodied carbon emissions of lettuce production in vertical farming, greenhouse horticulture, and open-field farming in the Netherlands," *J. Clean. Prod.*, vol. 377, p. 134443, Dec. 2022, doi: 10.1016/j.jclepro.2022.134443.

[41] R. H. E. Hassanien, M. M. Ibrahim, A. E. Ghaly, and E. N. Abdelrahman, "Effect of photovoltaics shading on the growth of chili pepper in controlled greenhouses," *Heliyon*, vol. 8, no. 2, p. e08877, Feb. 2022, doi: 10.1016/j.heliyon.2022.e08877.

[42] A. Cañete, M. Amor, and L. Fuentes, "Supporting IoT applications deployment on edge-based infrastructures using multi-layer feature models," *J. Syst. Softw.*, vol. 183, p. 111086, Jan. 2022, doi: 10.1016/j.jss.2021.111086.

[43] S. J. Mamouri, X. Tan, J. F. Klausner, R. Yang, and A. Bénard, "Performance of an integrated greenhouse equipped with Light-Splitting material and an HDH desalination unit," *Energy Convers. Manag. X*, vol. 7, p. 100045, Sep. 2020, doi: 10.1016/j.ecmx.2020.100045.

[44] F. Maureira, K. Rajagopalan, and C. O. Stöckle, "Evaluating tomato production in open-field and high-tech greenhouse systems," *J. Clean. Prod.*, vol. 337, p. 130459, Feb. 2022, doi: 10.1016/j.jclepro.2022.130459.

[45] J. Muñoz-Liesa, M. Royapoor, E. Cuerva, S. Gassó-Domingo, X. Gabarrell, and A. Josa, "Building-integrated greenhouses raise energy co-benefits through active ventilation systems," *Build. Environ.*, vol. 208, p. 108585, Jan. 2022, doi: 10.1016/j.buildenv.2021.108585.

[46] R. Liu, M. Li, J. L. Guzmán, and F. Rodríguez, "A fast and practical one-dimensional transient model for greenhouse temperature and humidity," *Comput. Electron. Agric.*, vol. 186, p. 106186, Jul. 2021, doi: 10.1016/j.compag.2021.106186.

[47] G. Yu, S. Zhang, S. Li, M. Zhang, H. Benli, and Y. Wang, "Numerical investigation for effects of natural light and ventilation on 3D tomato body heat distribution in a Venlo greenhouse," *Inf. Process. Agric.*, p. S221431732200052X, Jun. 2022, doi: 10.1016/j.inpa.2022.05.006.

[48] W. Cai, R. Wei, L. Xu, and X. Ding, "A method for modelling greenhouse temperature using gradient boost decision tree," *Inf. Process. Agric.*, vol. 9, no. 3, pp. 343–354, Sep. 2022, doi: 10.1016/j.inpa.2021.08.004.

[49] T. Persson, A. Chaillou, and P. Huang, "Low temperature heating system for greenhouses based on enclosed water curtain and liquid foam insulation," *Sustain. Energy Technol. Assess.*, vol. 53, p. 102472, Oct. 2022, doi: 10.1016/j.seta.2022.102472.

[50] I. Ihoume, R. Tadili, N. Arbaoui, M. Benchrifa, A. Idrissi, and M. Daoudi, "Developing a multi-label tinyML machine learning model for an active and optimized greenhouse microclimate control from multivariate sensed data," *Artif. Intell. Agric.*, vol. 6, pp. 129–137, 2022, doi: 10.1016/j.aiia.2022.08.003.

[51] D. Katzin, S. van Mourik, F. Kempkes, and E. J. van Henten, "GreenLight – An open source model for greenhouses with supplemental lighting: Evaluation of heat requirements under LED and HPS lamps," *Biosyst. Eng.*, vol. 194, pp. 61–81, Jun. 2020, doi: 10.1016/j.biosystemseng.2020.03.010.

[52] B. Chokara and S. K. R. Jammalamadaka, "Hybrid models for computing fault tolerance of IoT networks," *TELKOMNIKA Telecommun. Comput. Electron. Control*, vol. 21, no. 2, p. 333, Apr. 2023, doi: 10.12928/telkomnika.v21i2.22429.

[53] K. A. M. Annuar, R. Mohamed, and Y. Yusof, "Investigation of temperature gradient between ambient air and soil to power up wireless sensor network device using a thermoelectric generator," *TELKOMNIKA Telecommun. Comput. Electron. Control*, vol. 20, no. 1, p. 185, Feb. 2022, doi: 10.12928/telkomnika.v20i1.22463.

[54] F. Kamaruddin, N. N. Nik Abd Malik, N. A. Murad, N. M. Abdul Latiff, S. K. S. Yusof, and S. A. Hamzah, "IoT-based intelligent irrigation management and monitoring system using arduino," *TELKOMNIKA Telecommun. Comput. Electron. Control*, vol. 17, no. 5, p. 2378, Oct. 2019, doi: 10.12928/telkomnika.v17i5.12818.

[55] K. Sekaran, M. N. Meqdad, P. Kumar, S. Rajan, and S. Kadry, "Smart agriculture management system using internet of things," *TELKOMNIKA Telecommun. Comput. Electron. Control*, vol. 18, no. 3, p. 1275, Jun. 2020, doi: 10.12928/telkomnika.v18i3.14029.

[56] P. Megantoro, S. A. Aldhama, G. S. Prihandana, and P. Vigneshwaran, "IoT-based weather station with air quality measurement using ESP32 for environmental aerial condition study," *TELKOMNIKA Telecommun. Comput. Electron. Control*, vol. 19, no. 4, p. 1316, Aug. 2021, doi: 10.12928/telkomnika.v19i4.18990.

[57] [57] S.-E. Chafi, Y. Balboul, M. Fattah, S. Mazer, M. El Bekkali, and B. Bernoussi, "Resource placement strategy optimization for IoT oriented monitoring application," *TELKOMNIKA Telecommun. Comput. Electron. Control*, vol. 20, no. 4, p. 788, Aug. 2022, doi: 10.12928/telkomnika.v20i4.23762.

[58] M.-S. V. Nguyen, T.-T. Nguyen, and D.-T. Do, "User grouping-based multiple access scheme for IoT network," *TELKOMNIKA Telecommun. Comput. Electron. Control*, vol. 19, no. 2, p. 499, Apr. 2021, doi: 10.12928/telkomnika.v19i2.16181.

[59] M. Esmail Karar, A.-H. Abdel-Aty, F. Algarni, M. Fadzil Hassan, M. A. Abdou, and O. Reyad, "Smart IoT-based system for detecting RPW larvae in date palms using mixed depthwise convolutional networks," *Alex. Eng. J.*, vol. 61, no. 7, pp. 5309–5319, Jul. 2022, doi: 10.1016/j.aej.2021.10.050.

[60] M. E. Karar, F. Alsunaydi, S. Albusaymi, and S. Alotaibi, "A new mobile application of agricultural pests recognition using deep learning in cloud computing system," *Alex. Eng. J.*, vol. 60, no. 5, pp. 4423–4432, Oct. 2021, doi: 10.1016/j.aej.2021.03.009.

[61] R. Liu, H. Wang, J. L. Guzmán, and M. Li, "A model-based methodology for the early warning detection of cucumber downy mildew in greenhouses: An experimental evaluation," *Comput. Electron. Agric.*, vol. 194, p. 106751, Mar. 2022, doi: 10.1016/j.compag.2022.106751.

[62] S. Vieira, W. H. Lopez Pinaya, and A. Mechelli, "Introduction to machine learning," in *Machine Learning*, Elsevier, 2020, pp. 1–20. doi: 10.1016/B978-0-12-815739-8.00001-8.

[63] I. H. Witten, E. Frank, M. A. Hall, and C. J. Pal, "Trees and rules," in *Data Mining*, Elsevier, 2017, pp. 209–242. doi: 10.1016/B978-0-12-804291-5.00006-4.

[64] D. Y. Setyawan, D. Yuliawati, W. Warsito, and W. Warsono, "Calibration of Geomagnetic and Soil Temperatur Sensor for Earthquake Early Warning System," *TELKOMNIKA Telecommun. Comput. Electron. Control*, vol. 16, no. 5, p. 2239, Oct. 2018, doi: 10.12928/telkomnika.v16i5.7592.

[65] K. Devi Thangavel, U. Seerengasamy, S. Palaniappan, and R. Sekar, "Prediction of factors for Controlling of Green House Farming with Fuzzy based multiclass Support Vector Machine," *Alex. Eng. J.*, vol. 62, pp. 279–289, Jan. 2023, doi: 10.1016/j.aej.2022.07.016.

[66] U. Ahmed, J. C.-W. Lin, G. Srivastava, and Y. Djenouri, "A nutrient recommendation system for soil fertilization based on evolutionary computation," *Comput. Electron. Agric.*, vol. 189, p. 106407, Oct. 2021, doi: 10.1016/j.compag.2021.106407.

[67] A. S. Barneze, J. Whitaker, N. P. McNamara, and N. J. Ostle, "Interactions between climate warming and land management regulate greenhouse gas fluxes in a temperate grassland ecosystem," *Sci. Total Environ.*, vol. 833, p. 155212, Aug. 2022, doi: 10.1016/j.scitotenv.2022.155212.

[68] N. Ida, *Engineering Electromagnetics*. Cham: Springer International Publishing, 2015. doi: 10.1007/978-3-319-07806-9.